ELSEVIER

Journal of Alloys and Compounds 270 (1998) 237–241

Journal of ALLOYS AND COMPOUNDS

A study on lattice parameters of martensite in $Ti_{50.5-x}Ni_{49.5}Zr_x$ shape memory alloys

S.F. Hsieh, S.K. Wu*

Institute of Materials Science and Engineering, National Taiwan University, Taipei, Taiwan 106, Republic of China

Received 13 December 1997; received in revised form 28 January 1998

Abstract

$Ti_{50.5-x}Ni_{49.5}Zr_x$ (x=5~20 at.%) shape memory alloys exhibit the characteristics of B2↔B19′ martensitic transformation and their transformation temperatures increase linearly with increasing Zr content. The lattice parameters of B19′ martensite in these alloys are determined by XRD, SADP of TEM and the Rietveld method. Experimental results show that all of the lattice parameters a and c, monoclinic angle β and unit cell volume V increase, but lattice parameter b decreases with increasing Zr content in $Ti_{50.5-x}Ni_{49.5}Zr_x$ alloys. The results of the Rietveld method indicate that the martensite of $Ti_{50.5-x}Ni_{49.5}Zr_x$ with $x \leq 10$ at.% has a structure similar to that of $Ti_{50}Ni_{50}$, but that of $Ti_{50.5-x}Ni_{49.5}Zr_x$ with $x \geq 15$ at.% may change in structure. © 1998 Elsevier Science S.A.

Keywords: $Ti_{50.5-x}Ni_{49.5}Zr_x$ shape memory alloys; Martensitic transformation; Lattice parameters; B19′(Ti,Zr)Ni phase; Multiphase Rietveld method

1. Introduction

The martensitic transformation of B2↔B19′ in TiNi binary shape memory alloys (SMAs) has attracted considerable attention for the past years. The structure of the parent phase of TiNi SMAs is a B2 ordered cubic [1,2] and that of the martensite phase is a B19′ monoclinic in which the space group is $P2_1/m$ and the lattice parameters are a=0.2889 nm, b=0.4210 nm, c=0.4622nm and β=96.8° [3–5]. It is reported that the martensitic transformation of $Ti_{50-x}Ni_{50}Cu_x$ SMAs with x=0~30 at.% is B2↔B19 or B2↔B19′ or B2↔B19↔B19′ depending on the Cu-content [6–8]. For example, the ternary $Ti_{50}Ni_{40}Cu_{10}$ alloy undergoes B2↔B19↔B19′ two-stage martensitic transformation [9,10]. Here, the structures of B2 and B19′ are similar to those of TiNi binary SMAs, but the structure of B19 is an orthorhombic martensite. Lo et al. [10] reported that, during the B19→B19′ in the $Ti_{50}Ni_{40}Cu_{10}$ SMA, the monoclinic angle β of B19′ martensite will increase with decreasing temperature, which indicates that the B19→B19′ transformation has the characteristic of the ''continuous transformation''.

It is well known that $Ti_{50}Ni_{50-y}X_y$ ternary shape memory alloys with X=Pd, Pt or Au have a Ms, the martensite starting transformation temperature, much higher than 100°C and exhibit a one-way shape memory effect [11–14]. However, the high cost of precious metals will limit the practical applications of these SMAs. For this reason, other ternary TiNiX SMAs with lower costs need to be investigated. Among them, the most prospective candidates are TiNiZr and TiNiHf ternary alloys with Zr and Hf replacing Ti in these alloys [15]. Meisner et al. [16] reported that the lattice parameters of martensitic phase B19′, by using the XRD method, are dependent on Zr content in $Ti_{50-x}Ni_{50}Zr_x$ SMAs with Zr content in the range of 1 to 20 at.% at room temperature. Three phases (Ti,Zr)Ni, $(Ti,Zr)_2Ni$ and λ_1 are observed in Ti-rich $Ti_{53-x}Ni_{47}Zr_x$ SMAs with the Zr content in the range of 5~20 at.% at room temperature [17]. Here, λ_1 phase is a TiNiZr ternary solid solution and the (Ti,Zr)Ni phase can exhibit the B2↔B19′ martensitic transformation with Ms higher than 100°C [17]. However, the lattice parameters of B19′ martensite changing with Zr content in these Ti-rich $Ti_{53-x}Ni_{47}Zr_x$ alloys have yet to be reported. In this study, martensitic transformation of another Ti-rich $Ti_{50.5-x}Ni_{49.5}Zr_x$ SMAs with x=5~20 at.% is studied. The effect of Zr content on lattice parameters of martensite in these alloys, by using the XRD, SADPs (selected area diffraction patterns) and multiphase Rietveld methods, is also investigated.

2. Experimental procedure

The conventional vacuum arc melting with tungsten

*Corresponding author. Fax: +886 22 3634562.

PII: S0925-8388(98)00368-5

electrode technique was employed to prepare $Ti_{50.5-x}Ni_{49.5}Zr_x$ (x=5, 10, 15, 20 at.%) alloys. The symbols Zr_5, Zr_{10}, Zr_{15} and Zr_{20} are hereafter used to denote specimens of $Ti_{45.5}Ni_{49.5}Zr_5$, $Ti_{40.5}Ni_{49.5}Zr_{10}$, $Ti_{35.5}Ni_{49.5}Zr_{15}$ and $Ti_{30.5}Ni_{49.5}Zr_{20}$ alloys, respectively. Titanium (99.9%), nickel (99.9%) and zirconium (99.8%), totaling about 100 g, were melted and remelted at least six times in an argon atmosphere. A pure titanium button was used and melted before melting the alloys as an oxygen getter. The mass loss during the melting was negligibly small. The as-melted buttons were homogenized holding at 950°C for 72 h in vacuum and furnace-cooled. The homogenized buttons were cut into several plates with a low speed diamond saw and annealed at 900°C for 2 h in vacuum and quenched in water. The acquired specimens were polished for DSC, XRD, EPMA and TEM examinations.

DSC measurement was conducted by a Dupont 2000 thermal analyzer equipped with a quantitative scanning system 910 DSC cell for controlled heating and cooling runs on a sample encapsulated in an aluminum pan. The temperature range of measurement was from 0 to 400°C with a scanning rate of 10°C min^{-1}. The X-ray analysis of annealed specimens were performed at room temperature by a Phillips X-ray diffractometer, using monochromated Cu Kα radiation and a fixed time (6 s), step scan (step width 0.04° in 2θ) technique. X-Ray diffraction patterns were refined and analyzed by the multiphase Rietveld method [18]. The model parameters in this method that may be refined include not only atom-positional, thermal, and site-occupancy parameters but also parameters for the background, lattice, instrumental geometrical–optical features, specimen aberrations and specimen reflection-profile-broadening agents such as crystallite size and microstrain. Multiple phases may also be refined simultaneously and comparative analysis of the separate overall scale factors for the phases offers what is probably the most reliable current method for quantitative phase analysis [19]. The computer program used in this analysis is RIETAN for the Rietveld method developed by F. Izumi [20]. TEM images and electron diffraction were carried out using a JEOL-100CXII electron microscope operated at 100 kV and equipped with a conventional double tilting stage. TEM specimens were prepared by electropolishing at 0°C with an electrolyte consisting of 20% H_2SO_4 and 80% CH_3OH by volume. The applied voltage of the electropolishing was 20 V.

3. Experimental results and discussion

Fig. 1 shows the experimental results of DSC measurements for annealed Zr_5, Zr_{10}, Zr_{15} and Zr_{20} alloys in both forward and reverse transformations. Peaks appearing in Fig. 1 are identified as being associated with the martensitic transformation of B2↔B19′ [15]. The transformation peak temperatures of these alloys are shown in Table 1. From Fig. 1, it is clear that the transformation peak temperatures rise linearly from 50 to 320°C with increasing Zr content. Therefore, based on the results of Fig. 1, a TiNiZr SMA with the desired transformation temperature can be obtained by carefully controlling its Zr content. The more detailed shape memory properties of $Ti_{50.5-x}Ni_{49.5}Zr_x$ alloys after different thermomechanical processes are reported in another paper [21].

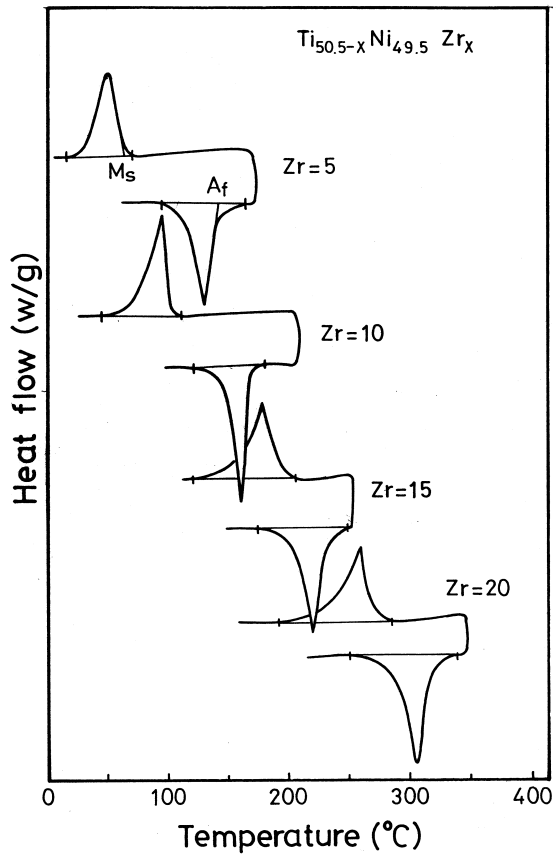

Fig. 1. DSC curves of homogenized $Ti_{50.5-x}Ni_{49.5}Zr_x$ (x=5~20 at.%) alloys. M_s and A_f are temperatures of forward and reverse martensite transformation, respectively.

A great number of second phase particles are seen around the grain boundaries in $Ti_{50.5-x}Ni_{49.5}Zr_x$ alloys with x=0~20 at.% and they are found to be $(Ti,Zr)_2Ni$, λ_1 and (Ti,Zr)Ni phases [21,22]. $(Ti,Zr)_2Ni$ and λ_1 phases do not transform martensitically within the temperature range

Table 1
The transformation peak temperatures of $Ti_{50.5-x}Ni_{49.5}Zr_x$ alloys

Zr (at.%)	A^* (°C)	M^* (°C)
5	120	54
10	152	84
15	217	176
20	306	260

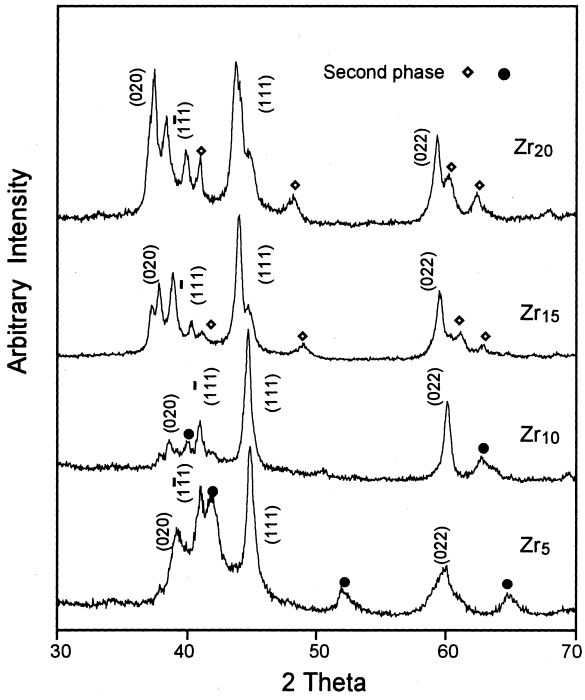

Fig. 2. X-Ray diffraction patterns of $Ti_{50.5-x}Ni_{49.5}Zr_x$ alloys.

described above. They are characterized by high brittleness and limited plasticity. For the (Ti,Zr)Ni phase, Fig. 2 shows its XRD spectra of (Ti,Zr)Ni phase from $\theta=30°$ to $\theta=70°$ for Zr_5, Zr_{10}, Zr_{15} and Zr_{20} alloys. By comparing these results with those of the B19′ martensite in the $Ti_{50}Ni_{50}$ alloy [5], lattice parameters of B19′ martensite can be calculated from the principal peaks $(020)_M$, $(1\bar{1}1)_M$, $(111)_M$ and $(022)_M$ shown in Fig. 2. Table 2 is the calculated lattice parameters a, b, c, β and the unit cell volume V of the B19′ martensite, where a, b, c are lattice constants and β is the monoclinic angle of the B19′ martensite. Fig. 3 shows the dependence of lattice parameters and volume of the B19′ phase on the Zr content of

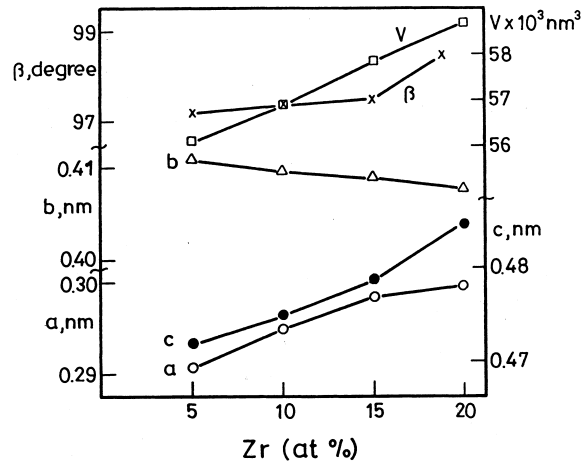

Fig. 3. Dependence of lattice parameters a, b, c, β and volume of unit cell V on Zr content of B19′ martensite in $Ti_{50.5-x}Ni_{49.5}Zr_x$ alloys.

$Ti_{50.5-x}Ni_{49.5}Zr_x$ alloys. As seen in this figure, parameters a, c, β and V increase while b decreases with increasing Zr content.

Fig. 4(a) shows the TEM bright field image of martensite in annealed Zr_{20} alloy. Fig. 4(b–d) are SADPs of Zr_5, Zr_{10} and Zr_{20} alloys, in which the foil normal is parallel to the $[100]_M$ direction. From Fig. 4(b–d), one can calculate the lattice parameters b and c and the results are shown in Table 2. From the TEM results of Table 2, we find that the tendency of lattice parameters b and c versus Zr-content in these alloys coincides with that of the XRD results.

Fig. 5(a,b) show the results of the multiphase Rietveld analysis method of annealed Zr_{10} and Zr_{20} alloys, respectively. In the upper curves of Fig. 5(a), the ''cross-marked'' line indicates the observed XRD data of Fig. 2 and the solid line indicates the pattern calculated by the multiphase Rietveld analysis method using the martensitic structure model (monoclinic B19′, the space group $P2_1/m$ [5]). The differences between the observed and calculated values are shown in the lower curve of Fig. 5(a). Fig. 5(a) indicates

Table 2
The lattice parameters and unit cell volume of B19′ martensite in $Ti_{50.5-x}Ni_{49.5}Zr_x$ alloys

Zr (at.%)	Parameter				
	a (nm)	b (nm)	c (nm)	β (degree)	$V\times10^3$ (nm^3)
By XRD profile of Fig. 2					
5	0.2916	0.4113	0.4718	97.20	56.14
10	0.2952	0.4094	0.4746	97.43	56.87
15	0.2976	0.4092	0.4790	97.53	57.83
20	0.2992	0.4080	0.4858	98.50	58.64
By SADP of TEM					
5	–	0.412	0.472	97.20[a]	–
10	–	0.408	0.481	97.43[a]	–
20	–	0.407	0.486	98.50[a]	–
By Rietveld method					
5	0.2921	0.4109	0.4707	97.35	56.03
10	0.2932	0.4081	0.4736	97.49	56.19

[a] Take data from XRD results.

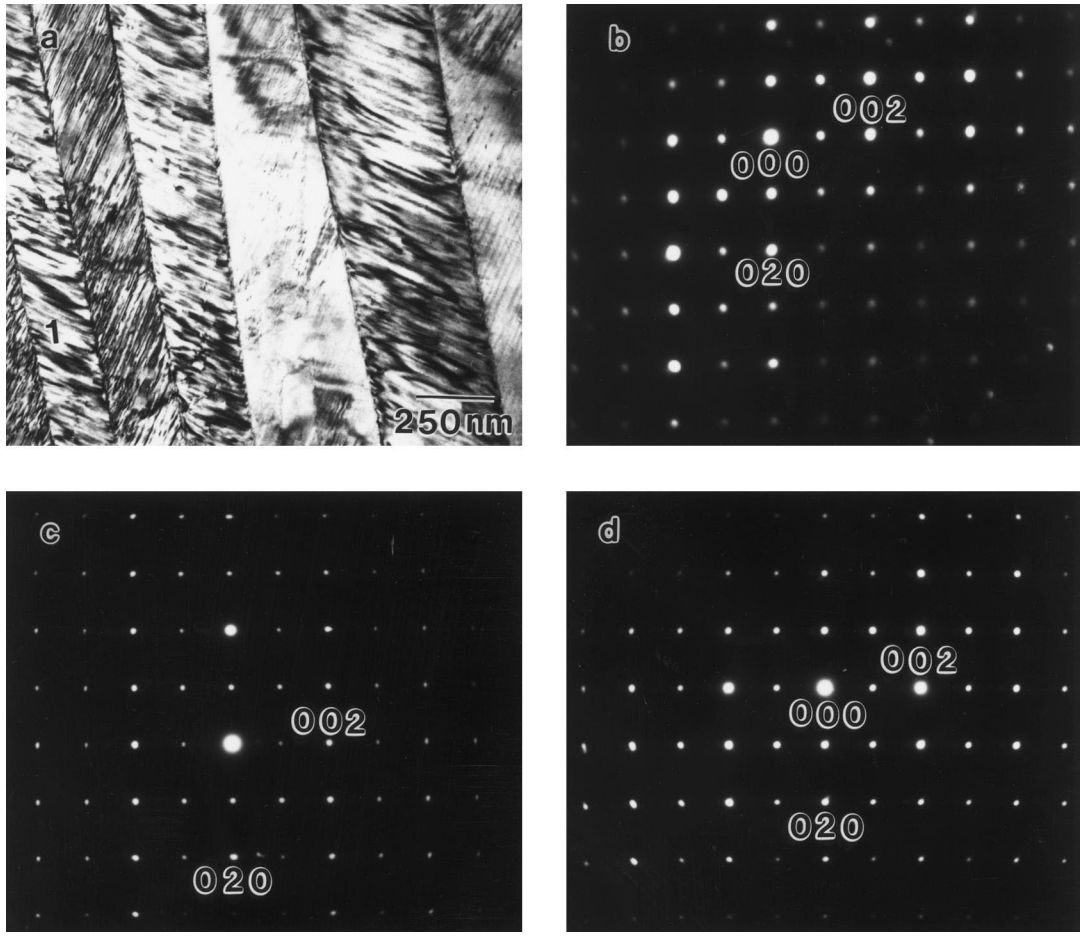

Fig. 4. (a) TEM bright-field image of martensite in $Ti_{30.5}Ni_{49.5}Zr_{20}$ alloy, (b), (c) and (d) are SADPs for Zr_5, Zr_{10} and Zr_{20} alloys, respectively. The zone axes are $[100]_M$.

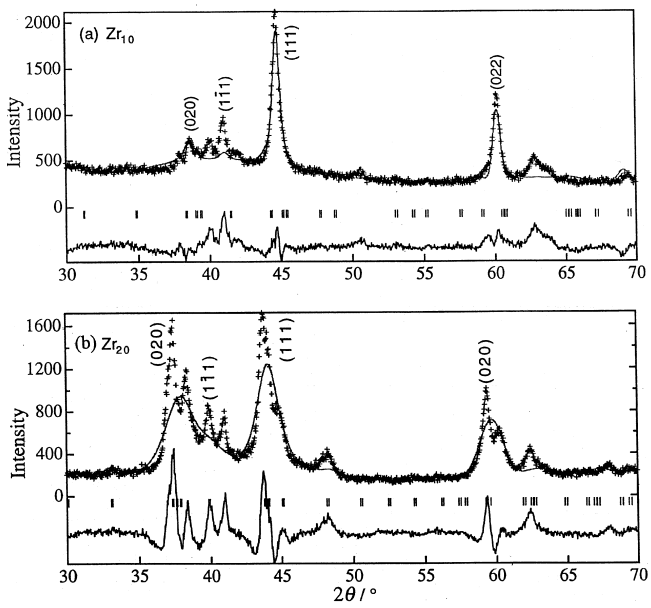

Fig. 5. Results of the Rietveld refinement for $P2_1/m$ model. Observed diffraction profile and calculated one for (a) Zr_{10}, (b) Zr_{20} alloys, respectively. In each figure, the lower curve stands for the deviation between observed and calculated intensities.

that the curve fitting of calculated peaks to observed ones, such as $(022)_M$, $(111)_M$, $(11\bar{1})_M$ and $(020)_M$ of Fig. 2, is rather good because the final reliability, R factor, R_{wp} is 13.28% and R_p is 10.17% which fall in the reasonable range (<15%) [23]. The subscript wp and p mean weighed pattern and pattern, respectively. Han et al. [24] found that lattice parameters of a monoclinic martensite in $Ti_{36.5}Ni_{48.5}Hf_{15}$ alloy are $a=0.293$ nm, $b=0.411$ nm, $c=0.473$ nm and $\beta=100.4°$. Therefore, it is reasonable to conclude that the space group of B19′ martensite for $Ti_{50.5-x}Ni_{49.5}Zr_x$ alloys with $x\leq 10$ at.% is still $P2_1/m$. Under this assumption, the lattice parameters calculated by the Rietveld method for Zr_5 and Zr_{10} alloys have nearly the same values as those calculated from XRD and TEM results, as shown in Table 2. Fig. 5(b) shows that the curve fitting of calculated peaks to observed ones for the martensite in annealed Zr_{20} alloy is not so good because the final reliability, R factor, R_{wp} is 20.84% and R_p is 16.88%. We suggest that the crystal structure of martensite may change in Ti-rich $Ti_{50.5-x}Ni_{49.5}Zr_x$ alloys for $x\geq 15$ at.%. A further study on this structural change is being conducted now.

4. Conclusion

1. $Ti_{50.5-x}Ni_{49.5}Zr_x$ (x=5~20 at.%) alloys exhibit martensitic transformation. The transformation temperatures Ms and As rise linearly from 50 to 320°C with increasing Zr content.
2. The lattice parameters of the B19′ martensite phase in these alloys are determined by XRD, SADP of TEM and the Rietveld method. Experimental results show that all of the lattice parameters a and c, monoclinic angle β and unit cell volume V increase, while lattice parameter b decreases with increasing Zr content in $Ti_{50.5-x}Ni_{49.5}Zr_x$ alloys. The results of the Rietveld method indicate that the martensite of $Ti_{50.5-x}Ni_{49.5}Zr_x$ with $x \leq 10$ at.% has a structure similar to that of $Ti_{50}Ni_{50}$, but that of $Ti_{50.5-x}Ni_{49.5}Zr_x$ with $x \geq 15$ at.% may change in structure.

Acknowledgements

The authors are pleased to acknowledge the financial support of this research by the National Science Council (NSC), Republic of China under Grant NSC 86-2216-E002-033. The valuable discussion with Dr. W.K. Chang, Institute of Materials Science and Engineering, National Taiwan University, in the calculation of the Rietveld method is highly appreciated.

References

[1] T.V. Philip, P.A. Beck, Trans. Am. Inst. Min. Eng. 209 (1957) 1269.
[2] G.M. Michael, P. Moine, R. Sinclair, Acta Metall. 30 (1982) 125.
[3] K. Otsuka, T. Sawamura, K. Shmizu, Phys. Status Solidi 5 (1971) 457.
[4] G.M. Michael, R. Sinclair, Acta Crystallogr. B 37 (1981) 1803.
[5] P. Villars, L.D. Calvert, Pearson's Handbook of Crystallographic Data for Intermetallic Phases, ASM International, Materials Park, OH, 1991, p. 4714.
[6] T. Tadaki, C.M. Wayman, Metallography 15 (1982) 233.
[7] T. Tadaki, C.M. Wayman, Metallography 15 (1982) 247.
[8] T. Saburi, T. Kamatsu, S. Nenno, Y. Watanabe, J. Less-Common Metals 118 (1986) 217.
[9] T.H. Nam, T. Saburi, Y. Kawamura, K. Shimizu, Trans. Jpn. Inst. Metals 31 (1990) 262.
[10] Y.C. Lo, S.K. Wu, H.E. Horng, Acta Metall. 41 (1993) 747.
[11] V.P. Sivokha, V.N. Khachin, Phys. Met. Metall. 62 (1986) 534.
[12] V.N. Khachin, N.M. Matveeva, V.P. Sivokha, Doklady AN SSSR 257 (1981) 167.
[13] V.P. Sivokha, A.S. Savionov, V.N. Khachin, Phys. Met. Metall. 56 (1983) 112.
[14] S.K. Wu, C.M. Wayman, Metallography 20 (1987) 359.
[15] J.H. Mulder, J.H. Mass, J. Beyer, Proc. of ICOMAT-92, 1992, p. 869.
[16] L. Meisner, V. Sivokha, J. Phys. IV (1995) C8–765.
[17] S.F. Hsieh, S.K. Wu, J. Alloys and Compounds, England, 1998 (in press).
[18] H.M. Rietveld, J. Appl. Crystallogr. 2 (1969) 65.
[19] R.A. Young, The Rietveld Method, International Union of Crystallography Oxford University Press, New York, 1995.
[20] F. Izumi, in: H. Saisho, Y. Gohshi (Eds.), Application of Synchrotron Radiation to Materials Analysis, Elsevier Science B.V., North-Holland Physics Publishing, Amsterdam, 1995, p. 405.
[21] S.F. Hsieh, Ph.D. thesis, Institute of Materials Science and Engineering, National Taiwan University, Taipei, Taiwan, 1997.
[22] V.N. Eremenko, E.L. Semenova, L.A. Tret′yachenko, Doklady AN Ukr. SSR, Ser. A 2 (1988) 76.
[23] W.K. Chang, Ph.D. thesis, Institute of Materials Science and Engineering, National Taiwan University, Taipei, Taiwan, 1996.
[24] X.D. Han, W.H. Zou, R. Wang, Z. Zhang, D.Z. Yang, K.H. Wu, J. Phys. IV (1995) C8–753.